Nonisothermal Crystallization Behavior and Mechanical Properties of Poly(butylene succinate)/Silica Nanocomposites

Junjia Bian, Lijing Han, Xuemei Wang, Xin Wen, Changyu Han, Shusheng Wang, Lisong Dong

State Key Laboratory of Polymer Physics and Chemistry, Changchun Institute of Applied Chemistry, Changchun 130022, China

Received 5 August 2009; accepted 11 October 2009
DOI 10.1002/app.31617
Published online 10 December 2009 in Wiley InterScience (www.interscience.wiley.com).

ABSTRACT: Silica nanoparticles and poly(butylene succinate) (PBS) nanocomposites were prepared by a melt-blending process. The influence of silica nanoparticles on the nonisothermal crystallization behavior, crystal structure, and mechanical properties of the PBS/silica nanocomposites was investigated. The crystallization peak temperature of the PBS/silica nanocomposites was higher than that of neat PBS at various cooling rates. The half-time of crystallization decreased with increasing silica loading; this indicated the nucleating role of silica nanoparticles. The nonisothermal crystallization data were analyzed by the Ozawa, Avrami, and Mo methods. The validity of kinetics models on the nonisothermal crystallization process of the PBS/silica nanocomposites is discussed. The approach developed by Mo successfully described the nonisothermal crystallization process of the PBS and its nanocomposites. A study of the nucleation activity revealed that the silica nanoparticles had a good nucleation effect on PBS. The crystallization activation energy calculated by Kissinger's method increased with increasing silica content. The modulus and yield strength were enhanced with the addition of silica nanoparticles into the PBS matrix. © 2009 Wiley Periodicals, Inc. J Appl Polym Sci 116: 902–912, 2010

Key words: crystallization; mechanical properties; nanocomposites

INTRODUCTION

In recent years, the development of biodegradable polymeric materials with excellent material properties has received much more attention worldwide.[1,2] Aliphatic polyesters, such as poly(ε-caprolactone), poly(lactic acid), poly(butylene succinate) (PBS), and poly(3-hydroxybutyrate), are among the most promising materials for the production of high-performance, environmentally friendly, biodegradable materials.[3–5] PBS, synthesized by the polycondensation of 1,4-butanediol with succinic acid, has particularly attracted increasing commercial interest because of its many interesting properties, including biodegradability, melt processability, and thermal and chemical resistance.[6]

However, its softness and low gas-barrier properties have restricted further application of PBS. To improve PBS's properties, the conventional method is to blend PBS with other materials.[7,8] The development of PBS-based nanocomposites has been an emerging method to improve PBS's properties, and many PBS-based nanocomposites have recently been developed for different applications. For example, Okamoto and coworkers[5,9] prepared PBS/layered silicate nanocomposites by melt compounding. The prepared PBS/layered silicate nanocomposites exhibited a concurrent improvement of materials properties when compared with pure PBS. Yoon and coworkers[10–12] synthesized and characterized a PBS/epoxy group functionalized organoclay nanocomposite and studied its nonisothermal crystallization kinetics. PBS/functional multiwalled carbon nanotube nanocomposites were prepared by melt compounding.[13] It was found that the presence of functional multiwalled carbon nanotube nanocomposites had a significant heterogeneous nucleation effect on the crystallization and morphology of PBS. Lim et al.[14] prepared PBS/silica nanocomposites to enhance the dispersability and interfacial adhesion between silica particles and the PBS matrix using the grafting method on a silica surface with PBS molecules. Moreover, PBS/silica nanocomposites were prepared by *in situ* polymerization.[15] The nanocomposites showed greatly improved mechanical and biodegradability properties. These improvements in the PBS properties were related to the crystallization behavior of the polymer.

Correspondence to: C. Han (cyhan@ciac.jl.cn).
Contract grant sponsor: Chinese Academy of Sciences; contract grant number: 0750221zz1.
Contract grant sponsor: National Science Foundation of China; contract grant number: 50703042.

The study of the nonisothermal crystallization behavior of thermoplastic polymers during nonisothermal processing is of great technical importance because most practical processing techniques are done under nonisothermal conditions. PBS is a semicrystalline polymer, and the final properties, such as thermal properties, impact resistance, stress–strain behavior, and biodegradable properties, of PBS-based nanocomposite in applications are critically dependent on the level of crystallinity, which, in turn, depends on the processing conditions. However, there has been little research related to the nonisothermal crystallization behavior of silica-nanoparticle-filled PBS nanocomposites.

In this study, the nonisothermal crystallization kinetics of PBS/silica nanocomposites, which were prepared by melt compounding at various silica contents, were investigated. The study of the nonisothermal crystallization kinetics, from differential scanning calorimetry (DSC) measurements, was performed with the Ozawa, Avrami, and Mo methods. The nucleation activity (ψ) and crystallization activation energy (ΔE_a) were also investigated. Finally, the effect of the silica nanoparticles on the mechanical properties of the PBS/silica nanocomposites was investigated by tensile testing.

EXPERIMENTAL

Materials and sample preparation

The PBS (AZ91TN) used in this study was a commercial product of Mitsubishi Chemical Corp. (Toyato, Japan) (trade name GS PLA, Japan). The melt flow index was 4.5 g 10/min at 190°C under 2.16 kg of weight. Silica (AEROSIL 200) was purchased from Degussa AG (Hanau, Germany), with a specific surface area of 200 m^2/g and an average primary particle size of 12 nm. Both PBS and silica were dried for 24 h at 80°C in a vacuum oven before use. PBS/silica nanocomposites were prepared with a Haake Rheomix (Karlsruhe, Germany) 600 internal mixer at various silica contents (1–10 wt %). The melt compounding was performed at 140°C for 5 min, the rotor speed was 50 rpm, and the total mixing weight per batch was 60 g. Then, the samples were hot-pressed at 140°C for 3 min and were then cold-pressed at room temperature to form films with thicknesses of 1 mm. For comparison, neat PBS was treated with the same procedure. The samples were abbreviated as PBS, PBS1, PBS3, PBS6, and PBS10 for 0, 1, 3, 6, and 10 wt % silica loadings in PBS, respectively.

Characterization

The morphology of the fractured surface, which was prepared under liquid N_2, was observed with a field emission scanning electron microscope (XL30 ESEM FEG, FEI Co., Eindhoven, The Netherlands) at an accelerating voltage of 15 kV. The fracture surface was coated with a thin layer of gold before the measurement.

The nonisothermal crystallization behavior of the neat PBS and PBS/silica nanocomposites was studied with a PerkinElmer (USA) DSC-7, and the weight of the sample was approximately 7 mg. The DSC instrument was calibrated with indium before the measurement. The samples were heated to 140°C at a heating rate of 10°C/min under a nitrogen atmosphere and held for 3 min to remove any previous thermal history. We investigated the nonisothermal crystallization kinetics by cooling these samples from 140 to 0°C at constant rates of 2.5, 5, 10, and 20°C/min.

Wide-angle X-ray diffraction (WAXD) patterns were recorded in the reflection mode at room temperature on a D8 Advance XRD (Bruker, Germany) automatic powder diffractometer with Ni-filtered Cu Kα radiation ($\lambda = 0.15418$ nm). The scans were obtained with a 0.1° step programmed with a collection time of 10 s per step. Measurements were performed in the range 5–45°.

For the determination of the mechanical properties, an Instron (USA) 1211 testing machine was used. The test was carried out at a crosshead speed of 20 mm/min at 25°C (room temperature). The values reported were averages for at least five dumbbell-shaped specimens with necks 20 mm long and cross-sectional areas of 4×1 mm^2.

RESULTS AND DISCUSSION

Morphological characterization

It is well known that the morphology and dispersion of silica nanoparticles in the polymer matrix are the key factors influencing the physical properties of the polymer matrix. A homogeneous dispersion of silica nanoparticles, together with strong interfacial interactions between the polymer matrix and silica nanoparticles, can effectively improve the thermal, mechanical, and rheological performances of the polymer matrix. To reveal the dispersion of silica nanoparticles in the PBS matrix, the fracture surfaces of the PBS/silica nanocomposites were investigated in detail by scanning electron microscopy (SEM). Figure 1 shows the SEM images of cross sections of the PBS/silica nanocomposites with various silica loadings. Generally, hydrophilic fumed silica easily aggregated because of the particle–particle interaction, and the aggregated silica nanoparticles were also found in the PBS/silica nanocomposites, as shown in Figure 1. Although the particle size of the fumed silica nanoparticles was only 12 nm, the size distribution of the silica nanoparticles ranged from

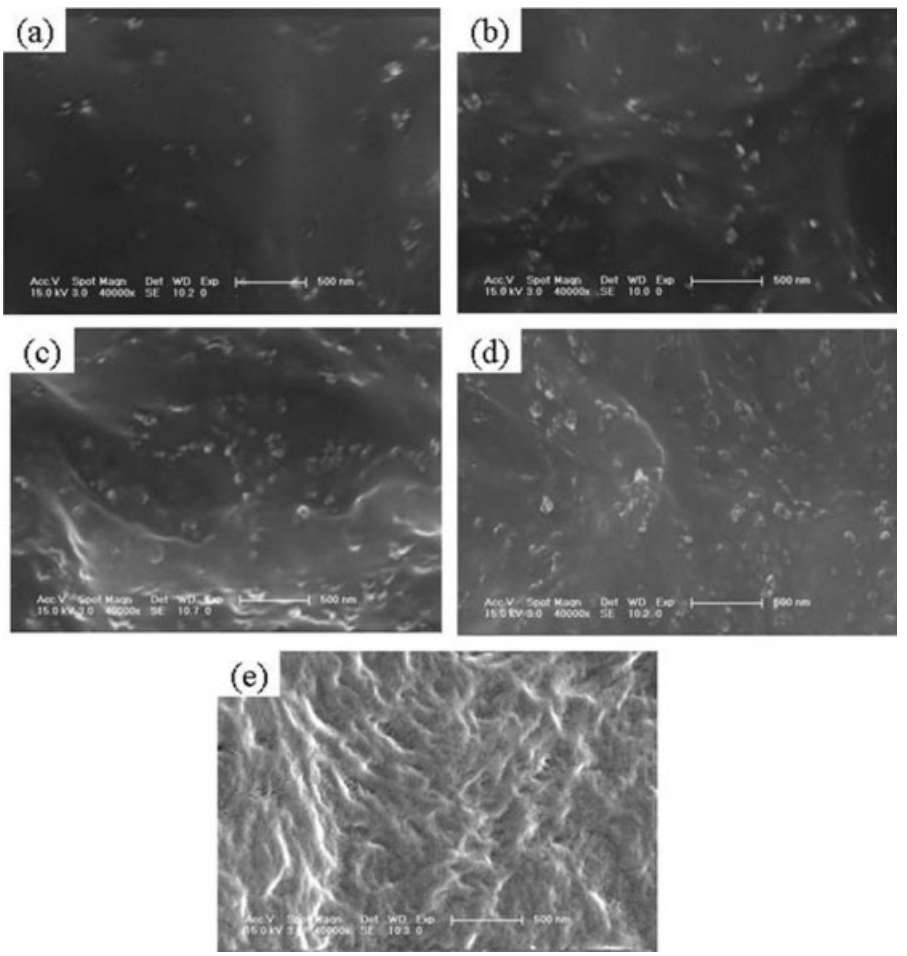

Figure 1 SEM microphotographs of the fractured surfaces of (a) PBS1, (b) PBS3, (c) PBS6, (d) PBS10, and (e) neat PBS.

tens of nanometers to 200 nm in the PBS matrix. However, the silica nanoparticles were dispersed evenly in the PBS matrix, even with 10 wt % loading, as a result of the sufficient shear force imposed during the melt-compounding process.

Nonisothermal crystallization behavior

The study of the nonisothermal crystallization behavior of thermoplastic polymers during nonisothermal processing is of great technical importance because most practical processing techniques are performed under nonisothermal conditions. The nonisothermal crystallization behaviors of neat PBS and its nanocomposites were investigated at cooling rates (α's) between 2.5 and 20°C/min. Figure 2(a,b) shows typical nonisothermal crystallization thermograms of the neat PBS and its nanocomposites. From these curves, some important nonisothermal crystallization parameters, such as the onset temperature of crystallization (T_o) and exothermic crystallization peak temperature (T_p), could be determined. These nonisothermal crystallization parameters, together with the enthalpy of crystallization (ΔH_c), are summarized and listed in Table I. ΔH_c was calculated from ΔH_c normalized to the PBS content. The percentage crystallinity (X_c) of neat PBS and its nanocomposites was determined by eq. (1), where the values of the heat of crystallinity of pure crystalline PBS (ΔH_c^o) was assumed to be 200 J/g:[6]

$$X_c = \Delta H_c / \Delta H_c^o \times 100\% \quad (1)$$

From DSC thermograms [Fig. 2(a,b) and Table I] at various α's (2.5, 5, 10, and 20°C), it was clear that T_p for the nanocomposites was higher than that of neat PBS and increased with decreasing α. The lower the α was, the higher the temperature at which the crystallization occurred. At a slower α, there was sufficient time to nucleate; therefore, the crystallization could occur at a higher temperature. For example, the crystallization temperature of PBS increased by 12.4°C in the presence of 1 wt % silica nanoparticles at an α of 2.5°C/min, whereas it decreased when α increased.

The curves, which show the variation of T_p with α for neat PBS and its nanocomposites, are shown in Figure 3. It was clear that T_p of the nanocomposites

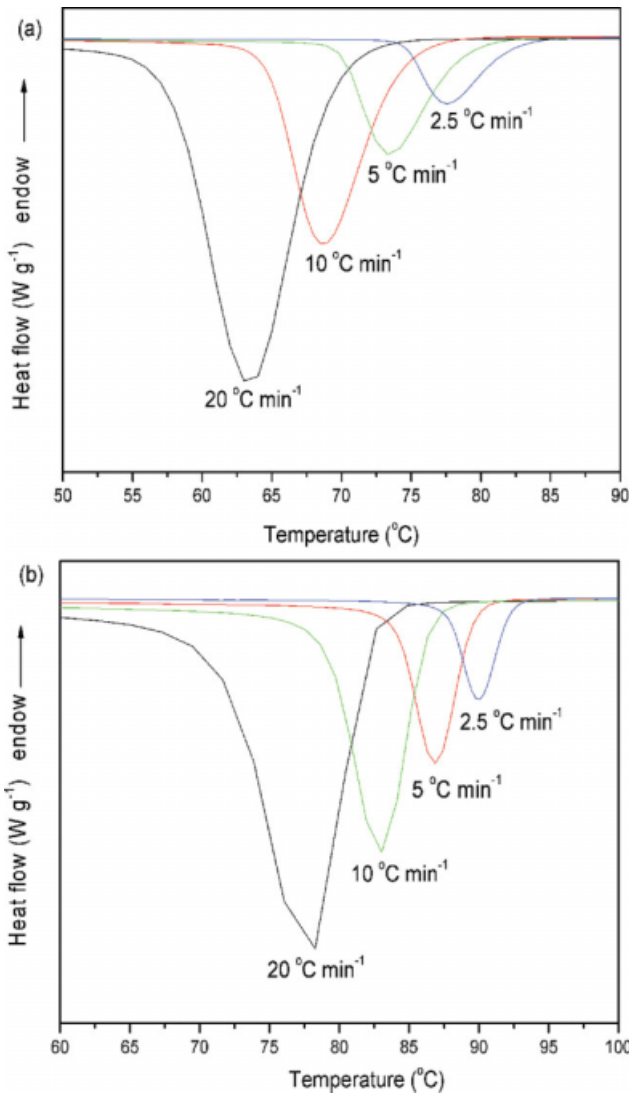

Figure 2 DSC thermograms of (a) PBS and (b) PBS1 during nonisothermal crystallization at various α's. [Color figure can be viewed in the online issue, which is available at www.interscience.wiley.com.]

was higher than that of the neat PBS at a given α. This phenomenon was attributed to the heterogeneous nucleation effect of the silica nanoparticles on the PBS matrix; this resulted in the crystallization of PBS taking place at a higher temperature.

Nonisothermal crystallization kinetics

From the DSC curves of melting crystallization, the values of relative crystallinity (X_T) at different α's as a function of temperature could be calculated according to eq. (2):

$$X_T = \frac{\int_{T_o}^{T} (dH_c/dT)dT}{\int_{T_o}^{T_\infty} (dH_c/dT)dT} \quad (2)$$

where T_o and T_∞ are the temperatures at which crystallization begins and ends H_c is the enthalpy of crystallization, and T is the crystallization temperature. The X_T values as a function of temperature for neat PBS and its nanocomposites at various α's are shown in Figure 4(a,b). The shape of the X_T versus T curves for PBS and its nanocomposites were very similar, and all of these curves exhibited the same sigmoidal shape.

During the nonisothermal crystallization process, the temperature could be related to crystallization time (t) according to eq. (3):

$$t = \frac{(T_o - T)}{\alpha} \quad (3)$$

where T is the temperature at time t. The results indicate that the lower the α was, the longer the time it took to complete crystallization. According to eq. (3), the value of T on the x axis could be transformed into t, as shown in Figure 5. From Figure 5, an important parameter that could be derived was the half-time of crystallization ($t_{1/2}$), which is defined as the half-period (i.e., 50% crystallization) from the onset of crystallization to the end of crystallization. The t and $t_{1/2}$ values of neat PBS and its nanocomposites are listed in Table I. It was clear that the value of $t_{1/2}$ decreased with increasing α. Moreover, at a given α, the $t_{1/2}$ value of the nanocomposites was lower than that of neat PBS. These results indicate that silica nanoparticles acted as heterogeneous nucleating agents to accelerate the overall crystallization process of the PBS/silica nanocomposites. A similar result was observed in the case of poly(ethylene 2,6-naphthalate)/silica nanocomposites.[16]

To further understand the development of crystallization during the nonisothermal crystallization process, the Ozawa, Avrami, and Mo (a combination of the Ozawa and Avrami methods) models were applied to analyze the nonisothermal crystallization kinetics of neat PBS and its nanocomposites.

The Ozawa theory[17] has been widely used to analyze the nonisothermal crystallization kinetics of polymers. According to Ozawa theory, X_T at a temperature T can be calculated from the following equation:

$$1 - X_T = \exp[-k(T)\alpha^m] \quad (4)$$

where $k(T)$ is a cooling crystallization function and m is the Ozawa exponent, which depends on the dimensions of crystal growth. The double logarithmic form of eq. (4) can be written as

$$\ln[-\ln(1 - X_T)] = \ln k(T) - m \ln \alpha \quad (5)$$

If the previous equation validly describes the nonisothermal crystallization kinetics, the plots of ln[−ln(1 − X_T)] against ln α should result in a straight line,

TABLE I
Nonisothermal Crystallization Parameters (ΔH_c, X_c, T_p, T_o, t, and $t_{1/2}$) for PBS and Its Nanocomposites at Various α's

Sample	α (°C/min)	ΔH_c (J/g)	X_c (%)	T_p (°C)	T_o (°C)	t (min)	$t_{1/2}$ (min)
PBS	2.5	59.7	29.9	77.6	86.5	8.04	3.390
	5	60.2	30.1	73.5	82.0	5.28	1.629
	10	59.2	29.6	68.7	78.5	2.54	0.941
	20	60.6	30.3	63.4	75.5	1.78	0.605
PBS1	2.5	59.6	29.8	90.0	95.0	7.58	2.065
	5	59.8	29.9	86.9	91.6	5.23	0.979
	10	59.3	29.7	82.9	88.5	2.55	0.603
	20	60.6	30.3	77.6	83.5	1.55	0.338
PBS3	2.5	58.8	29.4	90.4	94.2	6.25	1.554
	5	59.8	29.9	87.3	92.5	3.60	1.067
	10	59.0	29.5	83.5	88.4	2.09	0.504
	20	62.1	31.1	78.3	85.5	1.73	0.418
PBS6	2.5	58.9	29.5	90.4	96.0	5.65	2.244
	5	60.9	30.5	87.4	93.0	3.61	1.144
	10	62.4	31.2	83.7	90.0	2.42	0.650
	20	62.8	31.4	78.6	89.0	1.51	0.545
PBS10	2.5	60.1	30.1	90.3	95.5	5.45	2.160
	5	60.7	30.4	87.2	94.1	3.75	1.373
	10	63.9	32.0	83.3	89.9	2.65	0.677
	20	61.9	31.0	78.1	88.5	1.46	0.566

and the kinetic parameters $k(T)$ and m can be obtained from the intercept and the slope of the lines, respectively.

For PBS and PBS1, the Ozawa plots of $\ln[-\ln(1 - X_T)]$ against ln α at a given temperature are shown in Figure 6. As is evident from the figures, accurate analysis of the nonisothermal crystallization data could not be performed because the curves in the plots deviated from linearity, and an increase in curvature was observed. The nonisothermal crystallization process of PBS and its nanocomposites did not follow the Ozawa equation. The reason may have been the disregarded assumptions of slow secondary crystallization and the dependence of the fold length of the polymer chain on temperature in the Ozawa equation.[16]

An alternative approach for analyzing the time-dependent relative crystallinity function (X_t) for the nonisothermal crystallization process was the modified Avrami equation,[18] which can be expressed as

$$X_t = 1 - \exp(-Z_t t^n) \tag{6}$$

The previous equation can be liberated in its double logarithmic form to give eq. (7):

$$\ln[-\ln(1 - X_t)] = \ln Z_t + n \ln t \tag{7}$$

where n is the Avrami exponent, Z_t is the crystallization rate constant involving the nucleation and growth parameters, and X_t is the relative degree of crystallinity at time t. Avrami plots according to eq. (7), $\ln[-\ln(1 - X_t)]$ versus ln t for different α's, are shown in Figure 7. It was obvious that the initial stage of crystallization of PBS and its nanocomposites followed the Avrami equation and held in the region from the beginning of crystallization to the roll-off to a secondary process. The deviation of the Avrami plots may have been due to spherulite impingement, which indicated that there was a slow secondary crystallization that continued long after its boundary was formed.[19] The kinetic data in the initial linear regions were selected to estimate the Avrami parameters for the nonisothermal crystallization of PBS and its nanocomposites. The values of n and the rate parameter (Z_t) determined from the slope and intercept of the selected plots are shown in Table II. The n values were in the ranges 2.7–3.4 for neat PBS and 2.2–6.3 for the PBS/silica

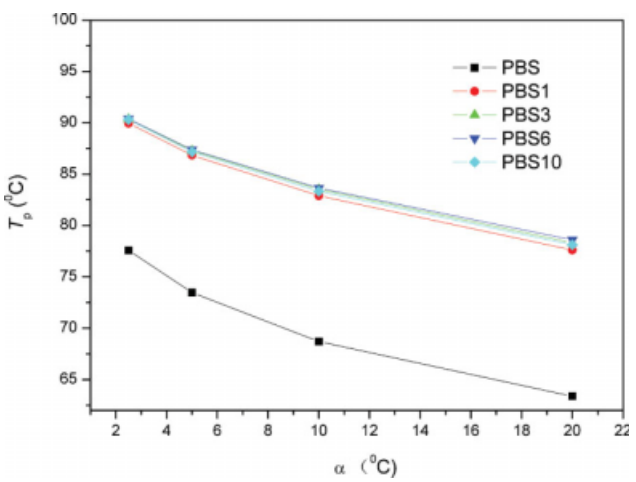

Figure 3 T_p versus α for PBS and its nanocomposites. [Color figure can be viewed in the online issue, which is available at www.interscience.wiley.com.]

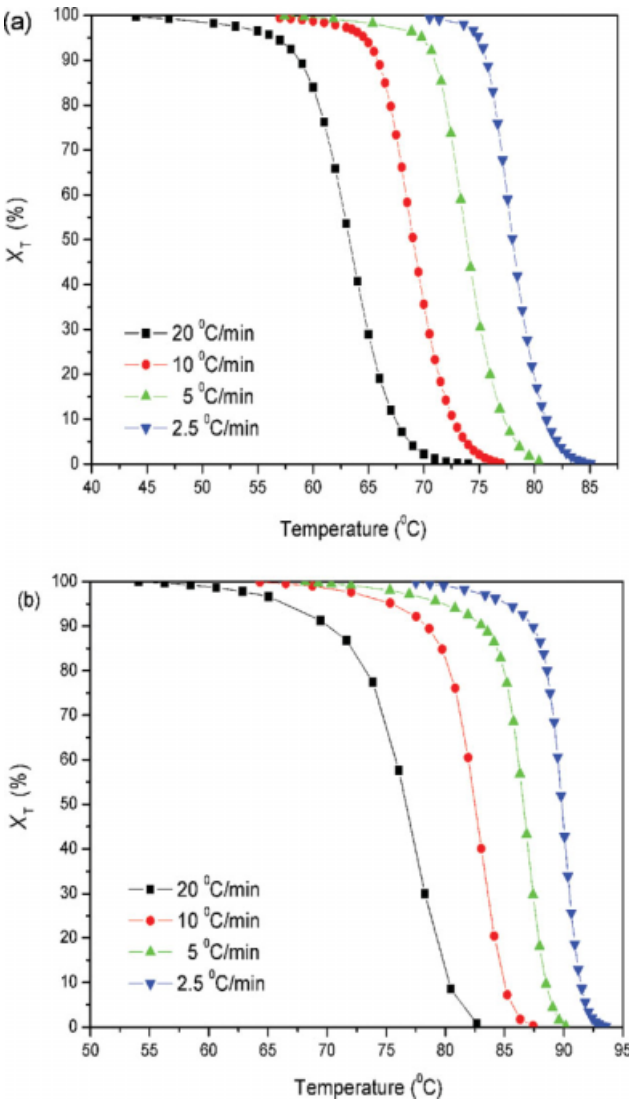

Figure 4 Relative crystallinity versus temperature for the nonisothermal crystallization of (a) PBS and (b) PBS1 at various α's. [Color figure can be viewed in the online issue, which is available at www.interscience.wiley.com.]

nanocomposites. As shown in Table II, the PBS6 and PBS10 samples exhibited values of n higher than 4. This result indicates that the nonisothermal crystallization mechanism of the PBS/silica nanocomposites with a relatively higher silica loading was very complicated; this suggested that the silica nanoparticles significantly affected both the mechanism of nucleation and the crystal growth of the PBS matrix. A similar result was also found by Kim et al.[20] in poly(ethylene 2,6-naphthalate)/multiwalled carbon nanotube nanocomposites.

From the previous analysis, it was evident that the Ozawa and modified Avrami models did not satisfactorily describe the nonisothermal crystallization process of neat PBS and its nanocomposites. There have been attempts to modify and combine these two basic models to study the nonisothermal crystallization process. In one such attempt, Mo et al.[21] proposed a convenient kinetic equation for describing nonisothermal crystallization kinetics by a combination of the Ozawa and Avrami equations; this was based on the assumption that the degree of crystallinity was correlated to α and t. Consequently, when eqs. (5) and (7) are combined, the kinetic model for the nonisothermal crystallization process can be derived as follows:

$$\ln Z_t + n \ln t = k(T) - m \ln \alpha \tag{8}$$

For a given crystallinity X_t, eq. (8) can be rewritten as

$$\ln \alpha = \ln F(T) - b \ln t \tag{9}$$

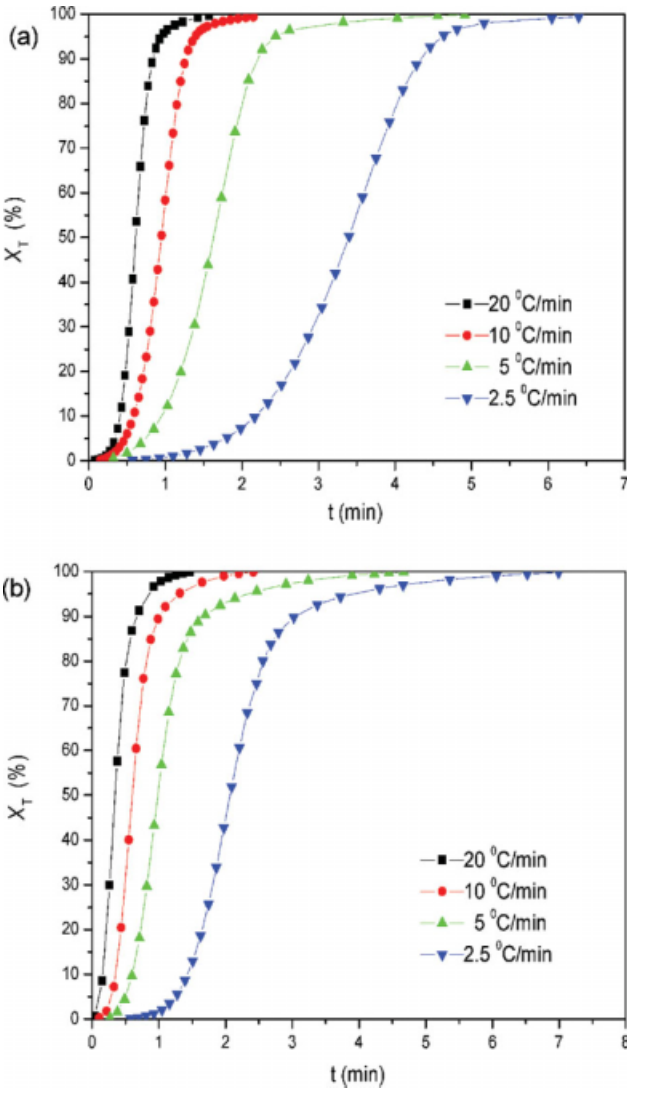

Figure 5 Relative crystallinity versus time for the nonisothermal crystallization of (a) PBS and (b) PBS1 at various α's. [Color figure can be viewed in the online issue, which is available at www.interscience.wiley.com.]

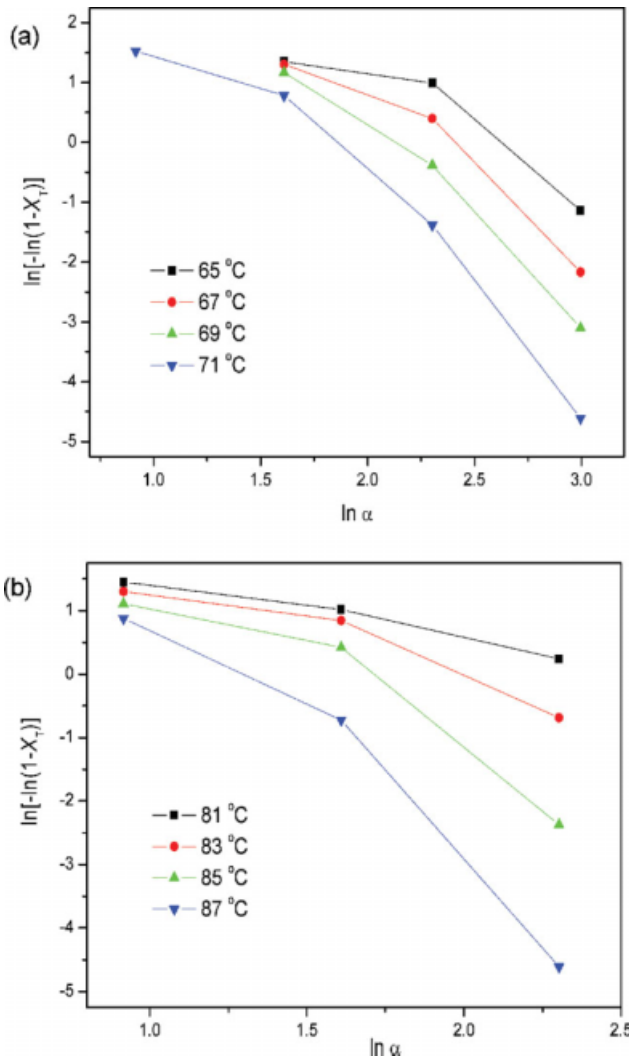

Figure 6 Ozawa plots of $\ln[-\ln(1 - X_T)]$ against $\ln \alpha$ for crystallization of (a) PBS and (b) PBS1. [Color figure can be viewed in the online issue, which is available at www.interscience.wiley.com.]

where $F(T) = [k(T)/Z_t]^{1/m}$ and refers to the value of α chosen at the unit of t when the system has a certain degree of crystallinity and b is the ratio of the n to m. According to eq. (9), at a given degree of crystallinity, the plot of $\ln \alpha$ against $\ln t$ should be a straight line. The kinetic parameters $F(T)$ and α can be calculated from the intercept and slope of the lines, respectively. Plots of $\ln \alpha$ against $\ln t$ for PBS and PBS1 are given in Figure 8. From Figure 8, it is clear that these plots exhibited relatively good linearity. The values for $F(T)$ and α calculated from the intercept and slope of the lines are listed in Table III. The values of α ranged from 1.17 to 1.20 for neat PBS and from 1.02 to 1.52 for the PBS/silica nanocomposites. For a given silica loading, the value of α increased with the relative degree of crystallinity. Almost all α values of neat PBS were lower than those of its nanocomposite at a given relative degree of crystallinity. The values of $F(T)$ increased with increasing relative degree of crystallinity and decreased in the PBS/silica nanocomposites; this indicated that the PBS/silica nanocomposites crystallized at a faster rate than PBS. Similar results were also reported for polypropylene/clay nanocomposithes,[22] polypropylene/layered double hydroxide nanocomposites,[23] poly(ethylene 2,6-naphthalate)/silica nanocomposites,[16] and poly(ethylene 2,6-naphthalate)/multiwalled carbon nanotube nanocomposites.[20]

ψ and activation energy

For the nonisothermal crystallization kinetics of polymers in the presence of nucleating agents, Dobreva and Gutzow[24,25] proposed a single method to calculate the nucleating activity of a foreign

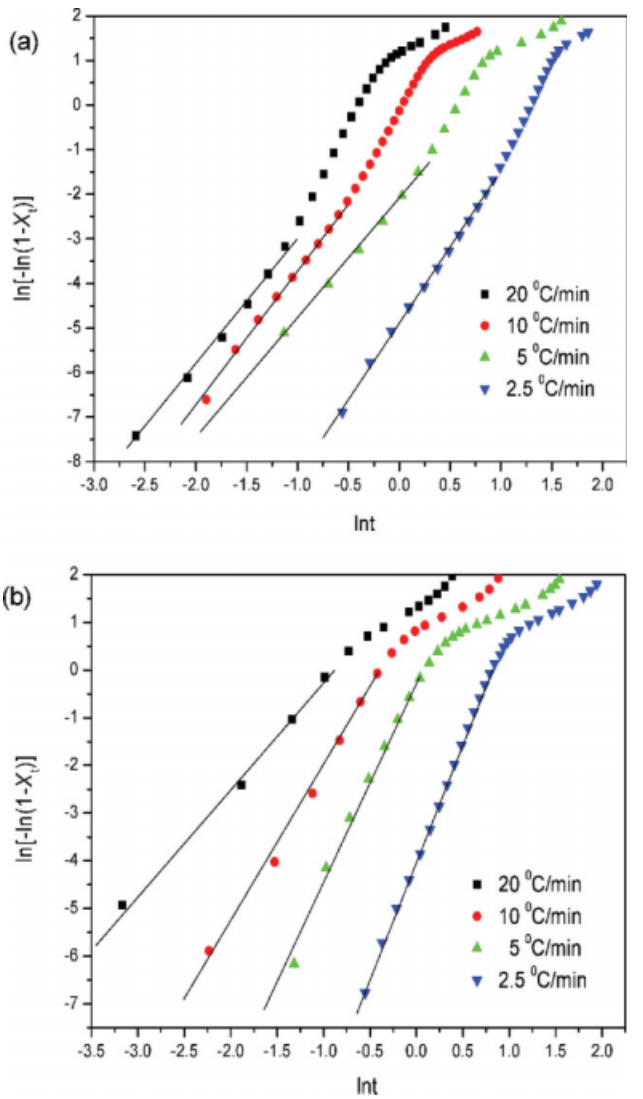

Figure 7 Avrami plots of $\ln[-\ln(1 - X_t)]$ against $\ln t$ for the crystallization of (a) PBS and (b) PBS1. [Color figure can be viewed in the online issue, which is available at www.interscience.wiley.com.]

TABLE II
Nonisothermal Crystallization Parameters Obtained by the Avrami Method

Sample	α (°C/min)	n	Z_t
PBS	2.5	3.4	0.0076
	5	3.0	0.1653
	10	3.2	0.65051
	20	2.7	0.60653
PBS1	2.5	5.0	0.01832
	5	4.2	0.81873
	10	3.2	3.32012
	20	2.2	6.68589
PBS3	2.5	3.7	0.14957
	5	3.9	0.49659
	10	2.6	3.6693
	20	3.8	29.9641
PBS6	2.5	6.3	0.00499
	5	5.0	0.36788
	10	3.8	3.00417
	20	6.0	29.9641
PBS10	2.5	4.1	0.0302
	5	6.1	0.1108
	10	4.1	22.19795
	20	6.1	36.59823

substrate in a polymer melt. ψ is a factor by which the three-dimensional nucleation process decreases with the addition of a foreign substrate. If the foreign substrate is extremely active for the nucleation, ψ approaches 0, whereas for an inert foreign substrate, ψ approaches 1. For homogeneous nucleation from a melt near the melting temperature, α is related to T_p and can be expressed as

$$\log \alpha = A - \frac{B}{2.3\Delta T_p^2} \tag{10}$$

Although for heterogeneous nucleation

$$\log \alpha = A - \frac{B^*}{2.3\Delta T_p^2} \tag{11}$$

$$\psi = B^*/B \tag{12}$$

where A is a constant, ΔT_p is the degree of supercooling (i.e., $\Delta T_p = T_m - T_p$, where T_m is the melting temperature), and B and B^* are parameters that relate to three-dimensional nucleation and can be determined from the following equation:

$$B = \frac{\omega\sigma^3 V_m^2}{3nkT_m\Delta S_m^2 n} \tag{13}$$

where ω is a geometrical factor, σ is the specific energy, V_m is the molar volume of the crystallizing substance, ΔS_m is the entropy of melting, and k is the Boltzmann constant. Hence, ψ can be calculated from the ratio of the slope of the plot of log β against $1/\Delta T_p^2$ with and without the filler. Figure 9 shows plots of log β against $1/\Delta T_p^2$ for neat PBS and its nanocomposites. The ψ values of PBS1, PBS3, PBS6, and PBS10 were calculated to be 0.33, 0.31, 0.33, and 0.31, respectively. From these results, it was obvious that the silica loading showed little effect on ψ of the PBS/silica nanocomposites. In a previous study on poly(ethylene 2,6-naphthalate)/silica nanocomposites,[16] the ψ value was 0.71. Thus, we concluded that the silica nanoparticles in the PBS/silica nanocomposites showed a much higher ψ than they did in the poly(ethylene 2,6-naphthalate)/silica nanocomposites.

One can determine ΔE_a for nonisothermal crystallization by combining α with T_p according to a method proposed by Kissinger[26,27] as follows:

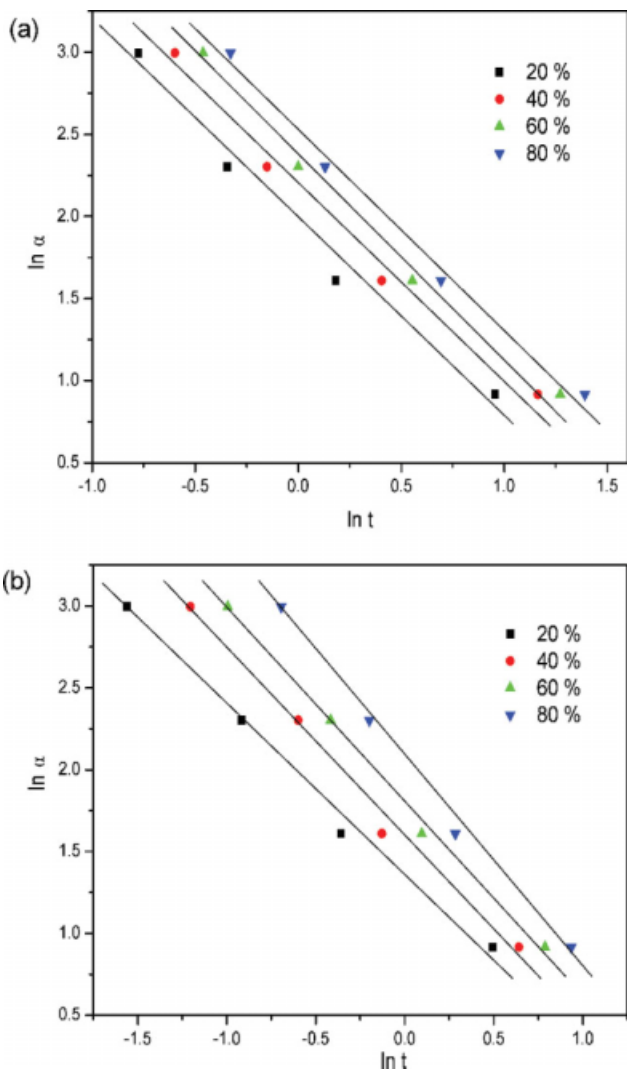

Figure 8 ln α versus ln t from the combined Avrami and Ozawa equation for (a) PBS and (b) PBS1. [Color figure can be viewed in the online issue, which is available at www.interscience.wiley.com.]

TABLE III
Kinetic Parameters for Neat PBS and Its Nanocomposites at Different Relative Degrees of Crystallinity by the Mo Method

Sample	X_T (%)	α	ln F(T)	ΔE_a (kJ/mol)
PBS	20	1.19	1.96	178.59
	40	1.17	2.20	
	60	1.19	2.36	
	80	1.20	2.52	
PBS1	20	1.02	1.36	217.82
	40	1.14	1.59	
	60	1.18	1.80	
	80	1.28	2.06	
PBS3	20	1.27	1.14	224.35
	40	1.34	1.45	
	60	1.42	1.69	
	80	1.48	1.96	
PBS6	20	1.32	1.58	229.94
	40	1.37	1.83	
	60	1.41	2.03	
	80	1.45	2.24	
PBS10	20	1.37	1.61	222.12
	40	1.39	1.87	
	60	1.45	2.09	
	80	1.52	2.31	

$$\frac{d[\ln(\alpha/T_p^2)]}{d(1/T_p)} = \frac{-\Delta E_a}{R} \quad (14)$$

where R is the universal gas constant. According to eq. (14), the crystallization activation energies of the nonisothermal crystallization for PBS and its nanocomposites are calculated from the slope of the plot of $\ln(\alpha/T_p^2)$ versus $1/T_p$, and the results are presented in Table III. It was clear that the crystallization activation energies of the PBS/silica nanocomposites were higher than that of neat PBS. Usually, ΔE_a reflects the crystallization ability of polymers. Polymers with higher ΔE_a values will exhibit lower crystallization abilities. The overall crystallization process involves both nucleation and growth. In the PBS/silica nanocomposites, the silica nanoparticles seemed to play two different or competing roles in affecting the crystallization process of PBS. One was that silica nanoparticles served as nucleating agents to accelerate the nonisothermal crystallization of the PBS/silica nanocomposites, as discussed earlier with regard to the nonisothermal crystallization kinetics. On the other hand, polymer chains were highly entangled in the melt state, and during crystallization process, the polymer chains had to overcome certain energy barriers to diffuse and attach onto the growing front of the crystal.[28] The presence of silica nanoparticles may have restricted the movement of chain segments and hindered the crystal growth process by imposing constraints upon the surrounding polymer chains,[28]

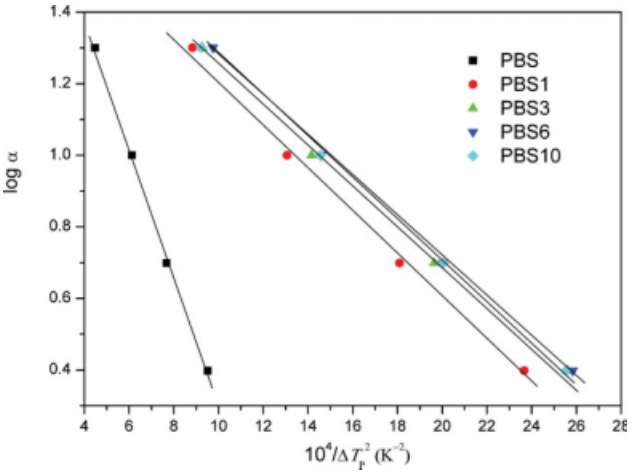

Figure 9 Plots of log α versus $1/\Delta T_p^2$ for neat PBS and its nanocomposites. [Color figure can be viewed in the online issue, which is available at www.interscience. wiley.com.]

especially when they had good interactions with the polymer chains. Therefore, the PBS molecular chains required more energy to rearrange; this resulted in an increment in the activation energy of nonisothermal crystallization. Similar results were also found for PBS/multiwalled carbon nanotube nanocomposithes.[28]

Crystal structure

It was of interest to study the effect of the incorporation of silica nanoparticles on the crystal structure of PBS in the nanocomposites. Figure 10 illustrates the WAXD patterns of neat PBS and its nanocomposites. As shown in Figure 10, neat PBS showed four main characteristic diffraction peaks around 19.54, 21.68,

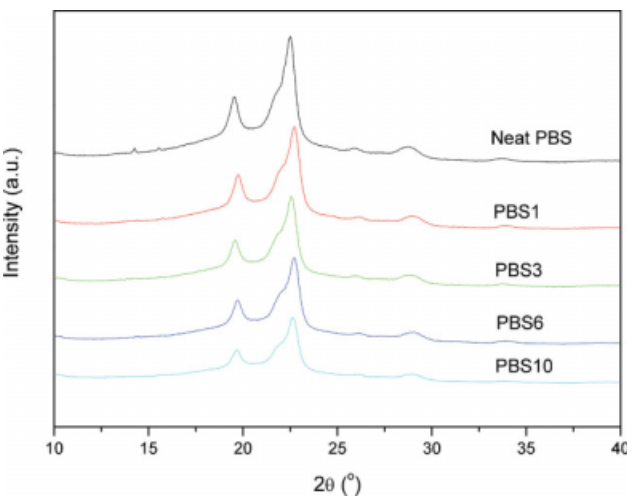

Figure 10 WAXD patterns of neat PBS and its nanocomposites. [Color figure can be viewed in the online issue, which is available at www.interscience.wiley.com.]

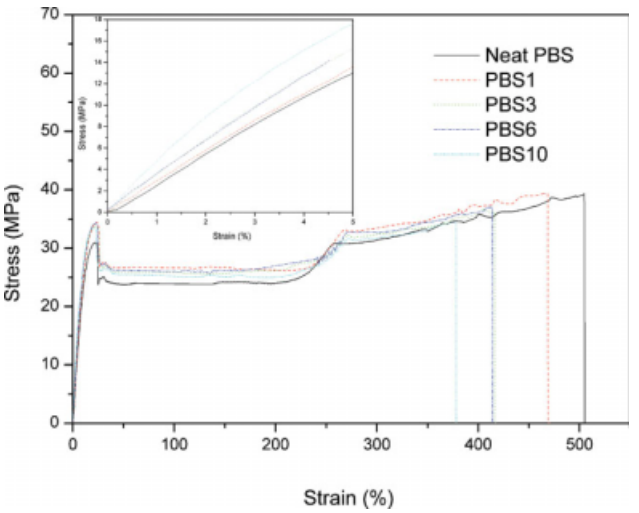

Figure 11 Stress–strain plots of neat PBS and its nanocomposites. Embedded figure: Elastic region for neat PBS and its nanocomposites. [Color figure can be viewed in the online issue, which is available at www.interscience.wiley.com.]

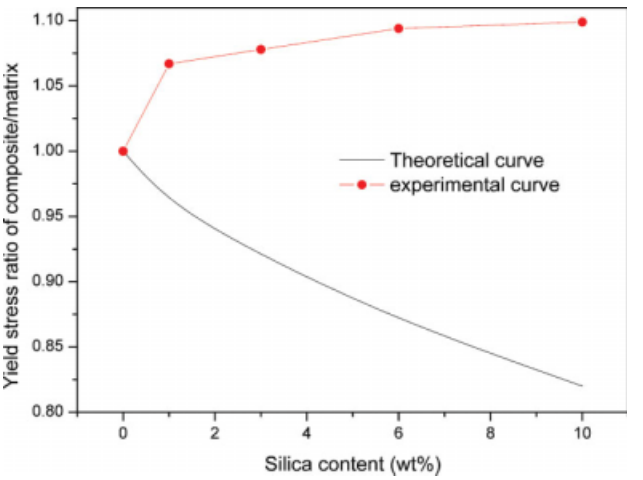

Figure 12 Effect of the silica content on the yield strength ratio of the composite and matrix. [Color figure can be viewed in the online issue, which is available at www.interscience.wiley.com.]

22.49, and 28.73°, corresponding to (020), (021), (110), and (111), respectively.[6] In the case of the nanocomposites, the diffraction peaks shifted slightly to a higher angle compared with those of neat PBS; this indicated that the incorporation of silica nanoparticles into the PBS matrix did not alter the crystal forms, and the corresponding interplanar spacings changed.

Mechanical properties

The effects of silica nanoparticles on the mechanical properties of the PBS/silica nanocomposites were investigated by tensile testing. Figure 11 shows the stress–strain plots of neat PBS and its nanocomposites. The data for tensile strength, elongation at break, modulus, and yield strength are summarized in Table IV. Neat PBS had a tensile strength of 38.9 MPa, an elongation at break of 498%, a modulus of 316 MPa, and a yield strength of 31.0 MPa. As shown in Table IV, the tensile strength and elongation at break of the nanocomposites decreased and the modulus and yield strength increased with increasing silica loading. Adhesion between the fillers and polymer matrix played an important role in affecting the mechanical properties of the composites. The improved modulus and yield strength of the PBS/silica nanocomposites indicated that stress transfers from the polymer matrix to stiffer fillers may have occurred. Thus, the Nichalais–Narkis model[29] was adapted to model theoretical tensile yield strength of the composites for the cases of adhesion and no adhesion between the filler and matrix as follows:

TABLE IV
Mechanical Properties of Neat PBS and Its Nanocomposites

Sample	Tensile strength (MPa)	Elongation at break (%)	Modulus (MPa)	Yield strength (MPa)
PBS	38.9 ± 0.7	498 ± 18	317 ± 24	31.0 ± 0.1
PBS1	38.0 ± 0.4	468 ± 3	371 ± 85	33.1 ± 1.3
PBS3	37.9 ± 0.3	447 ± 22	378 ± 91	33.4 ± 0.5
PBS6	37.1 ± 0.8	413 ± 35	392 ± 55	33.9 ± 0.4
PBS10	34.8 ± 0.7	375 ± 9	485 ± 21	34.1 ± 0.5

$$\delta_c = \delta_m(1 - a\varphi^b) \tag{15}$$

where φ, δ_c, and δ_m are the volume fraction of the filler and the tensile yield strengths of the composite and PBS matrix, respectively. Parameters a and b are constants related to the filler–matrix interaction and geometry of the filler, respectively. If there is good adhesion between the filler and polymer matrix, the values of a should be less than 1.21, whereas for the absence of adhesion, eq. (15) can be presented as follows:

$$\delta_c/\delta_m = (1 - 1.21\varphi^{2/3}) \tag{16}$$

The experimental and theoretical curves are plotted in Figure 12. It was obvious that the experimental value of the PBS/silica nanocomposites was much higher than that determined by eq. (16). This indicated that there was adhesion between the PBS matrix and the silica nanoparticles. All of the elongation of the composites arose from the polymer matrix because the silica nanoparticles were more rigid than the PBS matrix. Hence, increasing the amount of filler decreased the amount of polymer available

for elongation and thus decreased the elongation at break.[30]

CONCLUSIONS

Silica nanoparticle-filled PBS nanocomposites were prepared by a melt-blending process. The nonisothermal crystallization behavior of neat PBS and its nanocomposites containing 1–10 wt % silica was investigated by DSC. The kinetic studies indicated that the addition of silica nanoparticles into PBS led to a decrease in $t_{1/2}$ for various α's. This behavior was attributed to the nucleating effect of the silica nanoparticles. Kinetic models based on Ozawa, Avrami, and Mo were adapted to analyze the nonisothermal crystallization behavior of neat PBS and its nanocomposites; the former two models were inapplicable to satisfactorily describe the nonisothermal crystallization behavior of neat PBS and its nanocomposites. However, the method proposed by Mo and coworkers successfully described the nonisothermal crystallization behavior of neat PBS and its nanocomposites. ψ of the nanocomposites revealed that silica nanoparticles had a strong nucleation effect on PBS. The activation energy for the nonisothermal crystallization of the PBS/silica nanocomposites determined by the Kissinger method was higher than that of neat PBS because of the fact that the presence of silica nanoparticles may have restricted the movement of chain segments and hindered the crystal growth process by imposing constraints upon the surrounding polymer chains. Furthermore, the tensile strength and elongation at break of the nanocomposites decreased whereas the modulus and yield strength increased with increasing silica loading.

References

1. Pan, P. J.; Inoue, Y. Prog Polym Sci 2009, 34, 605.
2. Gorrasi, G.; Vittoria, V.; Murariu, M.; Ferreira, A.; Alexandre, M.; Dubois, P. Biomacromolecules 2008, 9, 984.
3. Avella, M.; Errico, M. E.; Laurienzo, P.; Martuscelli, E.; Raimo, M.; Rimedio, R. Polymer 2000, 41, 3875.
4. Witte, P.; Dijkstra, P. J.; Berg, J. W.; Feijen, J. J Polym Sci Part B: Polym Phys 1996, 34, 2553.
5. Ray, S. S.; Okamoto, K.; Okamoto, M. Macromolecules 2003, 36, 2355.
6. Song, J. B.; Song, C. L.; Wang, S. Y.; Zhang, H. F.; Mo, Z. S. Polym Int 2004, 53, 1773.
7. Dean, K.; Yu, L.; Bateman, S.; Wu, D. Y. J Appl Polym Sci 2007, 103, 802.
8. John, J.; Mani, R.; Bhattacharya, M. Polym Eng Sci 2002, 40, 2003.
9. Okamoto, K.; Ray, S. S.; Okamoto, M. J Polym Sci Part B: Polym Phys 2003, 41, 3160.
10. Chen, G. X.; Kim, H. S.; Yoon, J. S. Polym Int 2007, 56, 1159.
11. Chen, G. X.; Yoon, J. S. J Polym Sci Part B: Polym Phys 2005, 43, 817.
12. Chen, G. X.; Kim, E. S.; Yoon, J. S. J Appl Polym Sci 2005, 98, 1727.
13. Song, L.; Qiu, Z. B. Polym Degrad Stab 2009, 94, 632.
14. Lim, J. S.; Hong, S. M.; Kim, D. K.; Im, S. S. J Appl Polym Sci 2008, 107, 3598.
15. Han, S.; Lim, J. S.; Kim, D. K.; Kim, N. M.; Im, S. S. Polym Degrad Stab 2008, 93, 889.
16. Kim, S. H.; Ahn, S. H.; Hirai, T. Polymer 2003, 44, 5625.
17. Ozawa, T. Polymer 1971, 12, 150.
18. Avrami, M. J Chem Phys 1940, 8, 212.
19. Kong, X. H.; Yang, X. N.; Li, G.; Zhao, X. G.; Zhou, E. L.; Ma, D. Z. Eur Polym J 2001, 37, 1855.
20. Kim, J. Y.; Park, H. S.; Kim, S. H. Polymer 2006, 47, 1379.
21. Liu, T.; Mo, Z.; Wang, S.; Zhang, H. Polym Eng Sci 1997, 19, 568.
22. Yuan, Q.; Awate, S.; Misra, R. D. K. Eur Polym J 2006, 42, 1994.
23. Lonkar, S.; Therias, S.; Caperaa, N.; Leroux, F.; Gardette, J. L.; Singh, R. P. Polymer 2009, 50, 1505.
24. Dobreva, A.; Gutzow, I. J Non-Cryst Solids 1993, 162, 1.
25. Dobreva, A.; Gutzow, I. J Non-Cryst Solids 1993, 162, 13.
26. Kissinger, H. E. J Res Natl Stand 1956, 57, 217.
27. Kissinger, H. E. J Therm Anal 1956, 57, 217.
28. Pramoda, K. P.; Linh, N. T.; Zhang, C.; Liu, T. X. J Appl Polym Sci 2009, 111, 2938.
29. Yu, J. G.; Wang, N.; Ma, X. F. Biomacromolecules 2008, 9, 1050.
30. Pan, P. J.; Liang, Z. C.; Cao, A. M.; Inoue, Y. Appl Mater Interfaces 2009, 1, 402.